

Tetrahedral Connection of ϵ -Keggin-type Polyoxometalates To Form an All-Inorganic Octahedral Molecular Sieve with an Intrinsic 3D Pore System

Zhenxin Zhang,[†] Masahiro Sadakane,^{*,‡,§} Toru Murayama,[†] Shoko Izumi,[†] Nobuhiro Yasuda,^{||} Norihito Sakaguchi,[⊥] and Wataru Ueda^{*,†}

[†]Catalysis Research Center, Hokkaido University, N-21, W-10, Kita-ku, Sapporo 001-0021, Japan

[‡]Department of Applied Chemistry, Graduate School of Engineering, Hiroshima University, 1-4-1 Kagamiyama, Higashi Hiroshima 739-8527, Japan


[§]JST, PRESTO, 4-1-8 Honcho, Kawaguchi, Saitama 332-0012, Japan

^{||}Japan Synchrotron Radiation Research Institute/SPring-8, 1-1-1 Kouto, Sayocho, Sayogun, Hyogo 679-5198, Japan

[⊥]High Voltage Electron Microscope Laboratory, Center for Advanced Research of Energy Conversion Materials, Hokkaido University, Sapporo 060-8626, Japan

Supporting Information

ABSTRACT: A new type of polyoxometalate-based porous material was successfully synthesized. The new material is the first fully inorganic Keggin-type polyoxometalate-based microporous material with intrinsically ordered open micropores and is the third member of the small family of octahedral molecular sieves (OMSs). Twelve MoO₆ or VO₆ octahedra surround a central VO₄ tetrahedron to form ϵ -Keggin polyoxometalate building blocks (ϵ -VMo_{9.4}V_{2.6}O₄₀) that are linked by Bi^{III} ions to form crystalline Mo–V–Bi oxide with a diamondoid topology. The presence of a tetrahedral shape of the ϵ -Keggin polyoxometalate building block results in arrangement of microporosity in a tetrahedral fashion which is new in OMSs. Owing to its microporosity, this Mo–V–Bi oxide shows zeolitic-like properties such as ion-exchange and molecule adsorption.



INTRODUCTION

Polyoxometalates (POMs) are anionic metal oxide clusters of early transition metals such as molybdenum, vanadium, and tungsten. These materials have been widely applied to various fields such as catalysis, photocatalysis, materials science, magnetism, biology, and medicine.^{1–6}

Crystalline solids based on POMs with porosity are of great interest, because properties of POMs such as redox and acidic properties can be combined with pore-based properties such as size selective sorption of molecules and ions. A classical example of porous POM materials was microporous and/or mesoporous cesium or ammonium salts of α -Keggin-type POMs.^{4,7–10} The porosity of the materials was derived from aggregation of nanometer-size crystallites of POMs, and the pores were present between the crystallites. Control of the pores was an important factor for enhancing catalytic activity of these materials.

Recently, new approaches to form porous POMs have attracted much attention. Mizuno's group successfully developed a method to use large cation molecules (macro-cations) to synthesize porous POMs. The large cation molecules, which were composed of three chromium cations and six organic carboxylate such as [Cr₃O{RCO₂}₆L₃]⁺ (L =

ligand), and POMs formed crystalline materials with intrinsic micropores in their crystal structure.^{11–16} Pore properties were tunable by selection of organic moiety, metals, and/or POMs, and selective adsorption and catalytic reaction in the pores have been achieved.

Another new approach is assembly of POMs to form microporous complex metal oxides.^{17–19} We have succeeded in synthesizing orthorhombic and trigonal Mo–V oxides by assembly of pentagonal [(Mo)Mo₅O₂₁]⁶⁻ polyoxomolybdate units of giant POMs, {Mo₁₃₂}²⁰ or {Mo₇₂V₃₀}²¹ with other MoO₆ and VO₆ octahedra. The microporosity of the materials resulted from 7-member-ring channels of octahedra. Thus formed Mo–V oxides were redox active and showed outstanding catalytic activity for selective oxidations of light alkanes,^{22–24} acrolein,²⁵ and alcohols.^{26,27} Furthermore, the microporous properties were reversibly tunable by redox treatment.²⁸ Recently, the orthorhombic Mo–V oxide was applied as high capacity electrode materials for rechargeable lithium batteries.²⁹

Received: September 8, 2013

Published: December 30, 2013

There have been a few reports on inorganic POM-based frameworks.^{30–32} Linking of POM units with metal ions formed the frameworks with internal spaces. However, some organic molecules and/or ions occupied the spaces and were difficult to remove, and the pore of these materials could not be opened.

Another example of POM-based frameworks was achieved by using POMs as building blocks for construction of metal organic frameworks (so-called POMOFs).^{4,33–36} In POMOF materials, the ϵ -isomer of Keggin-type POMs is an ideal building block because ϵ -Keggin POMs have a truncated tetrahedral shape (T_d) with four hexagonal faces that can coordinate to metal ions (capping metal ions), such as Ni, Cu, Co, Bi, and La, by three oxygen atoms on one of the hexagonal faces (Figure 1).^{36–40} The capping metal ions can be

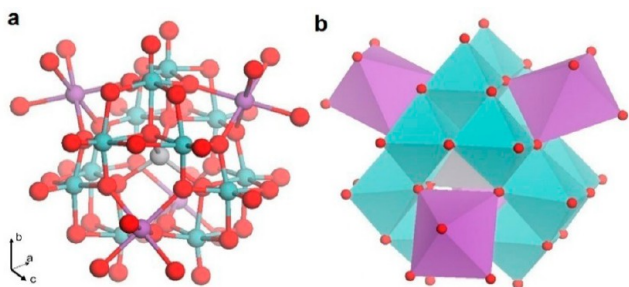


Figure 1. Representations of ϵ -VMo_{9.4}V_{2.6}O₄₀ Keggin core with capping Bi^{III} ions: (a) ball-and-stick representation and (b) polyhedron representation. Central V: gray. Bi: purple. Mo or V: blue. O: red.

coordinated by multidentate organic ligands that bridge the ϵ -Keggin POMs to form POMOFs.³⁴ However, the organic linkers result in materials with low oxidative and thermal stabilities, and the materials therefore cannot survive under harsh conditions.³⁴ Thus, no porosity was found in POMOFs due to molecules occupying the pores that cannot be removed without framework collapse.³⁴ A more inventive way would be to use metal ions to bridge ϵ -Keggin POMs without any organic linkers. So far, no example has been reported following this strategy.

Here, we report the first all-inorganic microporous material based on ϵ -Keggin-type POM (ϵ -VMo_{9.4}V_{2.6}O₄₀, designated as Mo–V–Bi oxide), in which intrinsic micropores can be opened. These POM units are connected by Bi^{III} ions to form a three-dimensional (3D) network. Mo–V–Bi oxide has a 3D pore system like FAU zeolite (Faujasite)⁴¹ and shows zeolitic-like properties such as selective molecule adsorption, ion-exchange, and catalysis.

Moreover, Mo–V–Bi oxide contained mostly octahedral coordinating metals and can be called “octahedral molecular sieves (OMSs)”. Two kinds of OMSs have been reported, the family of microporous Todorokite-type Mn and Fe oxides^{42,43} and Mo–V mixed oxides,^{19,28} and both of these have one-dimensional channels as with MTW-type (ZSM-12) zeolite.⁴⁴ Mo–V–Bi oxide is the third member of OMSs, and the 3D pore system is new in OMS materials.

EXPERIMENTAL SECTION

Material Preparation. (NH₄)₆Mo₇O₂₄·4H₂O (8.828 g, 50 mmol based on Mo) was dissolved in 110 mL of water. VOSO₄·5H₂O (3.219 g, 12.5 mmol) was dissolved in 110 mL of water. After the solids had been dissolved, the solution of VOSO₄·5H₂O was poured into the solution of (NH₄)₆Mo₇O₂₄·4H₂O. After the mixture was stirred at room temperature for 3 min, Bi(OH)₃ (0.438 g, 1.67 mmol) was

added. Then, the mixture was stirred for 7 min followed by N₂ bubbling for 10 min. The mixture was introduced into a 300-mL Teflon liner of a stainless-steel autoclave with the help of 20 mL of water. A Teflon sheet (4 m × 0.1 m × 0.1 mm) was inserted into the liner. The autoclave was placed in an oven heated at 448 K for 48 h. After the autoclave had been cooled down, the black solid on the bottom of the liner was transferred into centrifuge tubes with the help of water (200 mL) and separated by centrifugation (2000 rpm, 3 min). The collected solids were dispersed in water (200 mL) and separated by centrifugation (2000 rpm, 3 min). This washing process was repeated 6 times. The obtained solid was dried at 353 K overnight, and 0.45 g of Mo–V–Bi oxide (yield: 3.3% based on Mo) was obtained. FT-IR (KBr pellets, ν/cm^{-1}): 1620, 1402, 991, 955, 856, 813, 718, 698, 642, and 546 cm^{-1} . Anal. Calcd for Bi₂Mo_{9.4}V_{3.6}N_{2.8}O_{47.2}H_{26.5}: Bi, 17.98; Mo, 38.80; V, 7.89; N, 1.68; H, 1.15. Found: Bi, 18.45; Mo, 38.41; V, 7.51; N, 1.66; H, 0.97.

Ion-Exchange. As-synthesized Mo–V–Bi oxide (0.3 g) was dispersed in 15 mL of water that contained KCl (0.0455 g), LiCl (0.0259 g), NaCl (0.0367 g), RbCl (0.074 g), or CsCl (0.103 g). The mixture was stirred at 353 K for 6 h. The resulting solids were collected by filtration, washed with water (3 × 10 mL), and dried at 353 K overnight. For ion-exchange with protons, 0.5 mL of HCl (36%) was dissolved in 14.5 mL of water, and 0.3 g of Mo–V–Bi oxide was added to the solution. The mixture was stirred for 6 h at 353 K. The solid was recovered by filtration, washed with water (3 × 10 mL), and dried at 353 K overnight. The ion-exchanged materials were designated as M–Mo–V–Bi oxide (M = H, Li, Na, K, Rb, or Cs).

Elemental Analysis. H–Mo–V–Bi oxide ((NH₄)_{2.1}H_{0.7}H_{0.9}[ϵ -VMo_{9.4}V_{2.6}O₄₀Bi₂]·7.2H₂O), Calcd for Bi₂Mo_{9.4}V_{3.6}N_{2.8}O_{47.2}H_{24.4}: Bi, 18.08; Mo, 39.00; V, 7.93; N, 1.27; H, 1.06. Found: Bi, 18.13; Mo, 39.11; V, 7.54; N, 1.29; H, 0.98.

Li–Mo–V–Bi oxide ((NH₄)_{2.6}Li_{0.2}H_{0.9}[ϵ -VMo_{9.4}V_{2.6}O₄₀Bi₂]·7.2H₂O), Calcd for Li_{0.2}Bi₂Mo_{9.4}V_{3.6}N_{2.6}O_{47.2}H_{25.7}: Bi, 18.00; Mo, 38.84; V, 7.90; Li, 0.06; N, 1.57; H, 1.11. Found: Bi, 18.55; Mo, 38.41; V, 7.68; Li, 0.05; N, 1.48; H, 0.94.

Na–Mo–V–Bi oxide ((NH₄)_{2.2}Na_{0.6}H_{0.9}[ϵ -VMo_{9.4}V_{2.6}O₄₀Bi₂]·7.2H₂O), Calcd for Na_{0.6}Bi₂Mo_{9.4}V_{3.6}N_{2.2}O_{47.2}H_{24.1}: Bi, 17.96; Mo, 38.75; V, 7.88; Na, 0.59; N, 1.32; H, 1.04. Found: Bi, 18.51; Mo, 38.69; V, 7.44; Na, 0.58; N, 1.05; H, 0.86.

K–Mo–V–Bi oxide ((NH₄)_{0.9}K_{1.9}H_{0.9}[ϵ -VMo_{9.4}V_{2.6}O₄₀Bi₂]·6.1H₂O), Calcd for K_{1.9}Bi₂Mo_{9.4}V_{3.6}N_{0.9}O_{46.1}H_{16.5}: Bi, 17.83; Mo, 38.47; V, 7.82 K, 3.17; N, 0.54; H, 0.70. Found: Bi, 18.03; Mo, 38.27; V, 7.42; K 3.15; N, 0.42; H, 0.67.

Rb–Mo–V–Bi oxide ((NH₄)_{0.7}Rb_{2.1}H_{0.9}[ϵ -VMo_{9.4}V_{2.6}O₄₀Bi₂]·7.2H₂O), Calcd for Rb_{2.1}Bi₂Mo_{9.4}V_{3.6}N_{0.7}O_{47.2}H_{18.1}: Bi, 16.95; Mo, 36.58; V, 7.44; Rb, 7.28; N, 0.40; H, 0.73. Found: Bi, 16.58; Mo, 37.21; V, 7.52; Rb 7.12; N, 0.20; H, 0.53.

Cs–Mo–V–Bi oxide ((NH₄)_{0.8}Cs_{2.0}H_{0.9}[ϵ -VMo_{9.4}V_{2.6}O₄₀Bi₂]·7.2H₂O), Calcd for Cs₂Bi₂Mo_{9.4}V_{3.6}N_{0.8}O_{47.2}H_{18.5}: Bi, 16.36; Mo, 35.31; V, 7.18; Cs, 10.41; N, 0.44; H, 0.73. Found: Bi, 16.81; Mo, 34.97; V, 6.89; Cs, 10.49; N, 0.21; H, 0.57.

Calcination. The synthesized Mo–V–Bi oxide (1 g) was placed in a glass tube in a furnace, heated at 2 K/min to 623 K under N₂ (50 mL/min), and then maintained for 2 h at 623 K.

Crystal Growth. Low concentration of the precursor, long synthesis time, and seed were applied to obtain a large single crystal for X-ray single crystal analysis. An aqueous solution (110 mL) of (NH₄)₆Mo₇O₂₄·4H₂O (7.062 g, 40 mmol based on Mo) was mixed with 110 mL of an aqueous solution of VOSO₄·5H₂O (2.575 g, 10 mmol). After the mixture was stirred at room temperature for 3 min, Bi(OH)₃ (0.438 g, 1.67 mmol) was added, and synthesized Mo–V–Bi oxide (100 mg) was added as a seed. Then, the mixture was stirred for 7 min followed by N₂ bubbling for 10 min. The mixture was introduced into a 300-mL Teflon liner of a stainless-steel autoclave with the help of 20 mL of water, and a Teflon sheet (4 m × 0.1 m × 0.1 mm) was inserted into the liner. The autoclave had been heated at 448 K for 96 h. After the autoclave was cooled down to room temperature, the black solid on the bottom of the liner was transferred into centrifuge tubes with the help of 200 mL of water and separated by centrifugation (2000 rpm, 3 min). The collected solids were

dispersed in water (200 mL) and separated by centrifugation (2000 rpm, 3 min.). This washing process was repeated six times, and the obtained solid was dried at 353 K overnight. The obtained solid was used as a seed again. After repeating this crystal growth procedure four times, the crystal of Mo–V–Bi oxide was large enough for single crystal analysis.

To obtain a large crystal of K–Mo–V–Bi oxide for single crystal analysis, the large crystal of as-synthesized Mo–V–Bi oxide (50 mg) was dispersed in 2.5 mL of water followed by addition of KCl (7.6 mg). The mixture was heated at 353 K for 6 h. The solid was recovered by centrifugation, washed with water three times, and dried at 353 K overnight.

Characterization. Redox titration: The concentration of KMnO_4 solution was determined by using $\text{H}_2\text{C}_2\text{O}_4 \cdot \text{H}_2\text{O}$ as a standard compound. $\text{H}_2\text{C}_2\text{O}_4 \cdot 2\text{H}_2\text{O}$ (0.1157 g) was dissolved in 30 mL of water, followed by acidification with 15 mL of 16% H_2SO_4 . Titration was performed at 343–358 K. The concentration of KMnO_4 was 0.04848 mol/L. Then, Mo–V–Bi oxide (0.2867 g) was dissolved in 40 mL of 50% of H_2SO_4 that was degassed by N_2 bubbling in a 100-mL beaker. A Horiba D-52 pH meter with a metal (ORP) electrode was used to detect the potential of the Mo–V–Bi oxide solution. The solution of Mo–V–Bi oxide was titrated with the standard solution of KMnO_4 at room temperature. Measured potential was plotted against amount of KMnO_4 solution. Molecule (CO_2 , CH_4 , C_2H_6 , and C_3H_8) adsorption was performed on Mo–V–Bi oxide by a BELSORP MAX (BEL Japan Inc.) sorption analyzer at 298 K. The samples were evacuated at 573 K for 2 h before the measurement. Nitrogen isotherms were obtained by a BELSORP MAX (BEL Japan Inc.) sorption analyzer at 77 K. Surface area was calculated by the BET method using an adsorption branch, and pore distribution was estimated by the SF method using an adsorption branch. The samples were evacuated at 573 K for 2 h before the measurement. Powder X-ray diffraction (XRD) patterns were obtained on RINT2200 (Rigaku) with $\text{Cu K}\alpha$ radiation (tube voltage 40 kV, tube current 20 mA). Scanning electron microscopy (SEM) images were obtained with an HD-2000 (HITACHI). Transmission electron microscopy (TEM) images were taken with a 200 kV TEM (JEOL JEM-2010F). Carbon was deposited on the sample prior to TEM observation to reduce charging-up of the sample. Fourier transform infrared spectroscopy (FT-IR) was carried out on a PARAGON 1000 (Perkin-Elmer). Thermal analysis (TG-DTA) was performed on Thermo Plus, TG8120 (Rigaku). Temperature-programmed desorption mass spectrometry (TPD-MS) measurements were carried out from 313 to 893 K at a heating rate of 10 K min^{-1} under helium (flow rate: 50 mL min^{-1}). The Mo–V–Bi oxide sample was set between two layers of quartz wool. A TPD apparatus (BELJAPAN, Inc.) equipped with a quadrupole mass spectrometer (M-100QA; Anelva) was used to detect NH_3 ($m/z = 16$), H_2O ($m/z = 18$), O_2 ($m/z = 32$), and N_2 ($m/z = 28$). X-ray photoelectron spectroscopy (XPS) was performed on a JPS-9010MC (JEOL). The spectrometer energies were calibrated using the C 1s peak at 284.8 eV. Elemental compositions were determined by an inductive coupling plasma (ICP-AES) method (ICPE-9000, Shimadzu). CHN elemental composition was determined at Instrumental Analysis Division, Equipment Management Center, Creative Research Institution, Hokkaido University.

Computer-Based Simulation. All computer-based simulation was performed using Materials Studio v 6.1.0 (Accelrys Software Inc.). Rietveld analysis⁴⁵ of a powder XRD pattern was performed using “Reflex” tool in Materials studio. The lattice parameter and pattern parameters were refined by Pawley refinement based on the structural data obtained by single crystal structure analysis. All peak indexes were listed in Supporting Information (Table S1). Connolly surfaces, solvent surfaces, free space of Mo–V–Bi oxide, and volume of an C_2H_6 molecule were simulated by “Atom Volume & Surfaces” program in Materials Studio. The diameters of the cage and the channel were estimated from the Connolly surfaces of the cage and the channel with Connolly radius of 1 Å, and the shortest values were presented.⁴⁶ The theoretical accessible space of Mo–V–Bi oxide (without ammonium cations and water) was obtained by solvent surface calculation with solvent radius of 1.4 Å.⁴⁶ The volume of an

C_2H_6 molecule was obtained by Connolly surface calculation with Connolly radius of 1 Å.

Single Crystal Analysis. Since the crystals that had been grown were still too small for the diffractometer in the laboratory system, data collection was performed on a high-precision diffractometer installed in the SPring-8 BL40XU beamline.^{47,48} The synchrotron radiation emitted from helical undulator was monochromated by using a Si(111) channel cut monochromator and focused with a Fresnel zone plate. A Rigaku Saturn724 CCD detector was used. The measurement was performed at 100 (2) K. An empirical absorption correction based on Fourier series approximation was applied. The data were corrected for Lorentz and polarization effects. The structure was solved by direct methods and refined by full-matrix least-squares (SHELX-97),⁴⁹ where the unweighted and weighted agreement factors of $R = \sum |F_o| - |F_c| / \sum |F_o|$ ($I > 2.00\sigma(I)$) and $wR = [\sum w(F_o^2 - F_c^2)^2 / \sum w(F_o^2)^2]^{1/2}$, respectively, were used. Position of K in the structure of K–Mo–V–Bi oxide was determined from differential Fourier map. Nitrogen atoms of ammonium cations were modeled as oxygen atoms because nitrogen atoms could not be distinguished from oxygen atoms. Oxygen atoms of water in Mo–V–Bi oxide were refined isotropically, and other atoms were refined anisotropically. Total amounts of water and ammonium cations estimated by elemental analysis were slightly larger than those obtained by single crystal structure analysis. This is because of the difference in the crystal sample and bulk sample. The sample for elemental analysis may contain surface waters. Crystallographic data of Mo–V–Bi oxide and K–Mo–V–Bi oxide were listed in Table 1.

Table 1. Crystallographic Data of Mo–V–Bi Oxide and K–Mo–V–Bi Oxide

	Mo–V–Bi oxide	K–Mo–V–Bi oxide
formula	$\text{H}_{14.10}\text{Bi}_2\text{Mo}_{9.4}\text{O}_{47.05}\text{V}_{3.6}$	$\text{H}_{10.07}\text{Bi}_2\text{K}_{1.7}\text{Mo}_{9.4}\text{O}_{45.03}\text{V}_{3.6}$
M_r	2270.19	2300.21
cryst syst	cubic	cubic
space group	$Fd\bar{3}m$	$Fd\bar{3}m$
a (Å)	19.662(3)	19.6850(6)
V (Å ³)	7600.9(18)	7627.9(4)
T (K)	100(2)	100(2)
Z	8	8
ρ_{calcd} (g cm ⁻³)	3.968	4.006
F_{000}	8273	8369
λ (Å)	0.830 77	0.831 12
μ (mm ⁻¹)	14.593	14.838
measured reflns	3748	10 887
unique reflns	372	430
$R1(I > 2\sigma(I))$	0.0580	0.0344
wR2(all data)	0.1552	0.0646
GOF	1.091	0.904

Anisotropic displacement ellipsoids were presented in the Supporting Information Figure S1. Metal–oxygen bond lengths, atom coordinates, and atom occupancies are summarized in Table 2 and Supporting Information Tables S2 and S3, respectively. CIF data are available in

Table 2. Metal–Oxygen Bond Lengths from Single Crystal Analysis of As-Synthesized Mo–V–Bi Oxide^a

	bond length of Mo–V–Bi oxide (Å)	bond length of K–Mo–V–Bi oxide (Å)
V1–O4	1.76(2)	1.719(9)
Bi2–O3	2.355(12)	2.335(6)
M3–O1	1.640(12)	1.674(6)
M3–O2	1.894(5)	1.906(3)
M3–O3	1.964(8)	1.980(4)
M3–O4	2.428(12)	2.454(6)

^aM includes V and Mo.

Supporting Information. CSD-425857 and CSD-426125 contain the crystallographic data for Mo–V–Bi oxide and K–Mo–V–Bi oxide (data available from CrysDATA@FIZ-Karlsruhe.de).

Catalytic Test, Catalyst Recovery, and Filtration Experiment.

For the catalytic test, the calcined Mo–V–Bi oxide (20 mg) and 10 mmol of benzyl alcohol were added to a reaction tube. Some cotton (50 mg) was set at the uppermost part of the tube to adsorb the water generated during the reaction. The reaction tube was heated at 403 K for 3 h. After the temperature had cooled to room temperature, the cotton was removed, and 4 mmol of tridecane and 10 mL of acetone were added to the reaction tube. The mixture was stirred at room temperature for 5 min. Yield, conversion, and selectivity were measured by GC-FID. For catalyst recovery, the catalyst was recovered by centrifugation (5 min, 3000 rpm), washed with 5 mL of acetone 3 times, and dried at 353 K overnight. For the filtration experiment, 20 mg of calcined Mo–V–Bi oxide, 10 mmol of benzyl alcohol, and 0.8 mmol of tridecane were added to a reaction tube. A 50 mg portion of cotton was set at the uppermost part of the tube to adsorb the water generated during the reaction. The reaction tube was heated at 403 K. After reaction for 45 min, the material was removed using a syringe with a disposable syringe filter unit (PTFE, 0.2 μm) when the solution was still hot, and the filtrate kept on reacting. The reaction was monitored by GC.

RESULTS AND DISCUSSION

Synthesis and Structural Characterization. Hydrothermal reaction of $(\text{NH}_4)_6\text{Mo}_7\text{O}_{24}\cdot 4\text{H}_2\text{O}$, $\text{VOSO}_4\cdot 5\text{H}_2\text{O}$, and $\text{Bi}(\text{OH})_3$ produced crystalline Mo–V–Bi oxide, the powder XRD pattern of which is presented in Figure 2a. SEM images

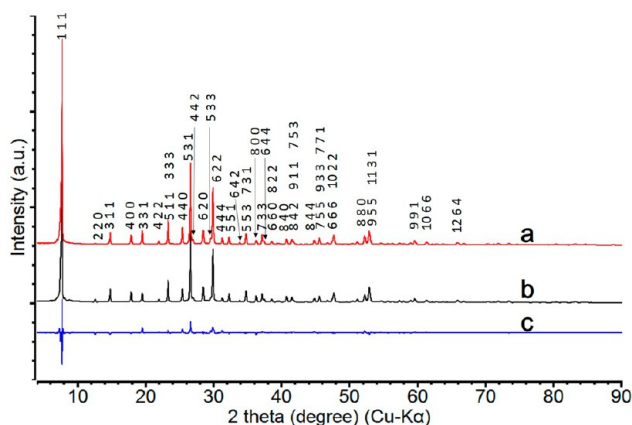


Figure 2. Comparison of (a) the experimental XRD pattern with (b) simulated pattern using structural data obtained by single crystal structure analysis with lattice parameter refinement ($a = 19.79 \text{ \AA}$, $R_{\text{wp}} = 10.49\%$), and (c) difference of experimental pattern and simulated pattern.

showed that the resulting solids were polyhedral crystals that were too small (less than 1 μm in one dimension) to perform single crystal structure analysis (Supporting Information Figure S2a). Therefore, crystal growth experiments were performed using the synthesized Mo–V–Bi oxide as a seed in the reaction mixture. After repeating the crystal growth procedure, crystals of Mo–V–Bi oxide large enough ($\sim 5 \mu\text{m}$ in one diameter) for single crystal analysis were obtained (Supporting Information Figure S2b).

Single crystal structure analysis and elemental analysis (Mo:V:Bi = 9.4:3.6:2) of the as-prepared Mo–V–Bi oxide and K-exchanged sample (designated as K–Mo–V–Bi oxide, with ion-exchange presented in a later section) revealed that the building block of Mo–V–Bi oxide was an ϵ -Keggin-type

polyoxovanadomolybdate, $\epsilon\text{-VMo}_{9.4}\text{V}_{2.6}\text{O}_{40}$, that was formed by one central VO_4 tetrahedron surrounded by 12 distorted MO_6 ($M = \text{Mo}$ or V) octahedra (Figure 1). The central atom of this POM was a 4-fold coordinated vanadium with bond length of V–O being 1.76(2) or 1.719(9) \AA for Mo–V–Bi oxide and K–Mo–V–Bi oxide, respectively. Bond valence sum (BVS) calculation revealed that valence of the central V was 5+, which is often observed in polyoxometalate compounds.^{40,50} Four edge-sharing M_3O_{13} ($M = \text{Mo}$ or V) units were anchored to this tetrahedral VO_4 to form the ϵ -Keggin POM. Disordering of the molybdenum and vanadium atoms in the surrounding 12 positions was detected, as has been often observed in polyoxomolybdates⁵¹ and Mo–V-based complex metal oxides.¹⁷ Three oxygen atoms in each hexagonal face of the POM coordinated to Bi, and an adjacent POM supplied three oxygen atoms in the hexagonal face to the Bi to form a diamond-like 3D framework (Figure 3). The bond length of Bi–O was 2.355(12) or 2.335(6) \AA for Mo–V–Bi oxide and K–Mo–V–Bi oxide, respectively, and BVS calculations revealed that the valence of the Bi linker was 3+.

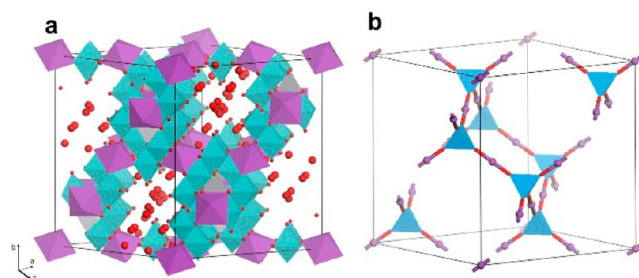


Figure 3. (a) Polyhedral representation of Mo–V–Bi oxide. Central V: gray. Bi: purple. Mo or V: light blue. O: red. (b) Schematic representation of Mo–V–Bi oxide, POM unit: blue tetrahedron, Bi: purple.

The powder X-ray diffraction pattern of Mo–V–Bi oxide was similar to the simulated pattern obtained by using crystal data from single crystal structure analysis (Figure 2). Furthermore, there were no additional peaks in the experimental data, indicating that the powder sample of Mo–V–Bi oxide was pure.

Figure 4 shows a comparison of the generated polyhedral image and the high-resolution transmission electron micro-

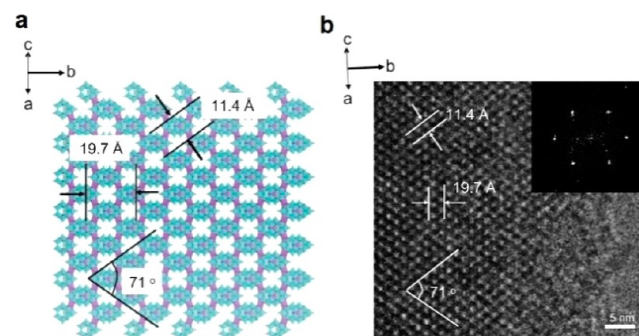


Figure 4. Comparison of polyhedron representation of Mo–V–Bi oxide with HRTEM. (a) Polyhedral representation and (b) HRTEM image (insert: power spectrum) of Mo–V–Bi oxide, viewed along the 101 direction. Mo–V–Bi oxide was not so stable under TEM condition, and an amorphous-like part was produced during observation.

copy (HRTEM) image of Mo–V–Bi oxide along the 101 direction. The HRTEM revealed a characteristic face-centered cubic lattice image for Mo–V–Bi oxide. Ordering of the rhombic black and white spots in the HRTEM image was exactly the same as the ordering of ϵ -VMo_{9.4}V_{2.6}O₄₀ building blocks and pores. The unit cell lengths and distances of the (111) plane were obtained from the HRTEM image: 19.7 Å and 11.4 Å, respectively.

The oxidation states of the metal elements were studied by X-ray photoelectron spectroscopy (XPS) (Figure 5), which indicated that reduced states of molybdenum (Mo^V) and vanadium (V^{IV}) existed, and the oxidation state of bismuth was 3+. Furthermore, XPS showed that 25% of the molybdenum and 50% of the vanadium were Mo^V and V^{IV}, respectively. The total reduced metal content (molybdenum and vanadium) was

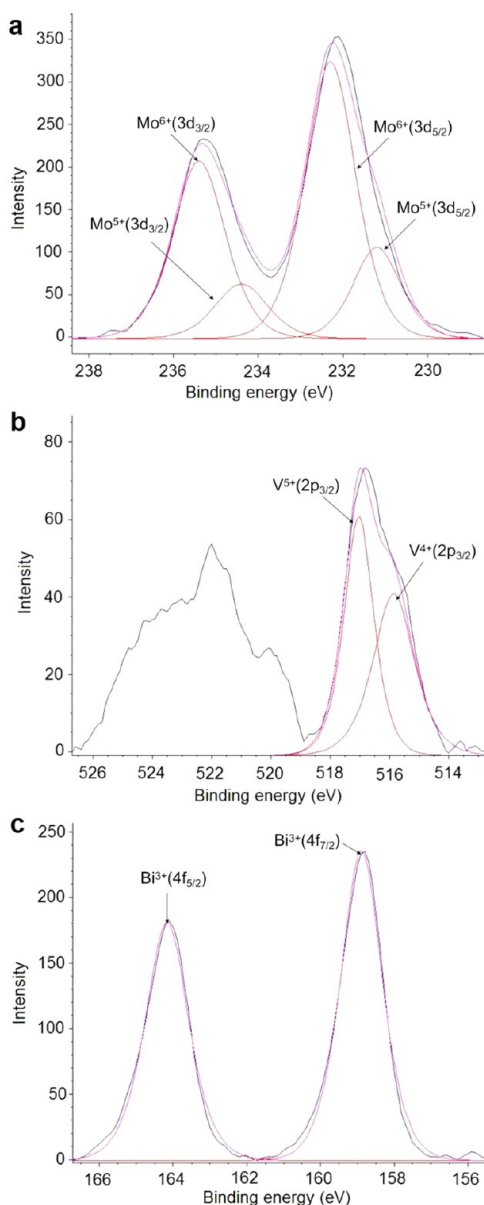


Figure 5. XPS and curve fitting results of Mo–V–Bi oxide of (a) molybdenum, Mo⁶⁺/Mo⁵⁺ = 3, (b) vanadium, V⁵⁺/V⁴⁺ = 1, and (c) bismuth. Blue: experimental data. Purple: sum of every simulated peak. Red: simulated peak.

32%. Manganometric redox titration also confirmed that ca. 28% of the total metal (molybdenum and vanadium) was reduced (Figure 6). Partial reduction was in good agreement with other reported ϵ -Keggin POM molecules. In the case of [ϵ -Mo^V₁Mo^V₁₂O₄₀(C₅M_eS_{Rh}^{III})₈]²⁺,⁵² [ϵ -P^VMo^V₈Mo^{VI}₄O₃₆(OH)₄{La^{III}(H₂O)₄]₄]⁵⁺,³⁸ and [ϵ -H₂Mo^V₁₂O₃₀(OH)₁₀{Ni^{II}(H₂O)₃]₄]³⁷, all or part of the surrounding 12 metal ions are reduced. Thus, the detailed formula of the ϵ -Keggin POM framework was [ϵ -V^V_{1.0}Mo^V_{2.3}Mo^{VI}_{7.1}V^{IV}_{1.8}V^V_{0.8}O₄₀Bi^{III}]₂.^{3,7}

There were cages and channels in Mo–V–Bi oxide. A cage was composed of 10 ϵ -VMo_{9.4}V_{2.6}O₄₀ building blocks that were connected by Bi^{III} ions (Figure 7a,b). The internal diameter of the cage was ca. 7.7 Å. One cage was tetrahedrally connected with four other adjacent cages by four channels (Figure 7c,d). The diameter of the channel was ca. 3.4 Å. The cages and channels constructed a periodical 3D pore system for Mo–V–Bi oxide in a tetrahedral fashion. In one direction, the tunnel of the micropore was not straight but in a zigzag-like fashion (Figure 7e and Supporting Information Figure S3), which is new in OMSs.

Single crystal structure analysis of Mo–V–Bi oxide revealed that there were two types of sites for water or NH₄⁺ (10 sites per one ϵ -VMo_{9.4}V_{2.6}O₄₀ unit). One was in the cage, and the other was in the channel. Nitrogen (represented NH₄⁺) could not be distinguished from oxygen (represented H₂O) by single crystal analysis (Figure 7e). An FT-IR spectrum (Supporting Information Figure S4a) of Mo–V–Bi oxide showed the presence of water (1620 cm⁻¹) and NH₄⁺ (1402 cm⁻¹) together with bands at 991, 955, 856, 813, 718, 698, 642, and 546 cm⁻¹, which were attributed to the framework. The amount of NH₄⁺ was estimated by elemental analysis to be ca. 2.8 for one ϵ -Keggin POM. Therefore, the detailed formula can be expressed as (NH₄)_{2.8}H_{0.9}[ϵ -V^V_{1.0}Mo^V_{2.3}Mo^{VI}_{7.1}V^{IV}_{1.8}V^V_{0.8}O₄₀Bi^{III}]₂·7.2H₂O.

The NH₄⁺ and H₂O in Mo–V–Bi oxide were removable by heat-treatment. TG-DTA of Mo–V–Bi oxide indicated that there were two weight losses: one was between ca. 310 and 490 K, and the other was between ca. 580 and 710 K (Supporting Information Figure S5). Temperature programmed desorption (TPD) analysis revealed that the first weight loss corresponded to desorption of water and NH₃ and that the second weight loss corresponded to desorption of water, NH₃, and N₂ (Supporting Information Figure S5). N₂ was produced by decomposition of NH₄⁺. Total weight loss from room temperature to 773 K was ca. 7.8%, which was in accord with the total amount of NH₄⁺ and water estimated by elemental analysis. TPD results showed that there were two kinds of NH₄⁺ in the material. One NH₄⁺, which had a strong interaction with the framework, desorbed at 633 K (peak top) and is denoted as NH₄⁺(S). The other, which had a relatively weak interaction with the framework, desorbed at 443 K (peak top) and is denoted as NH₄⁺(W). These results indicated that NH₄⁺ and water co-occupied two different positions in the as-synthesized material: one was in the cage, and the other was in the channel. Total NH₄⁺ amount estimated by TPD was slightly less than NH₄⁺ amount estimated by elemental analysis, because some NH₄⁺ were released as N₂ (Table 3, entry 1).

Microporosity. The NH₄⁺ and water were removed by calcination (2 K/min, 623 K for 2 h, N₂ flow rate of 50 mL/min) without structural collapse (Supporting Information Figure S6a,b). However, further heating (calcination at 673 K) caused the framework of Mo–V–Bi oxide to collapse

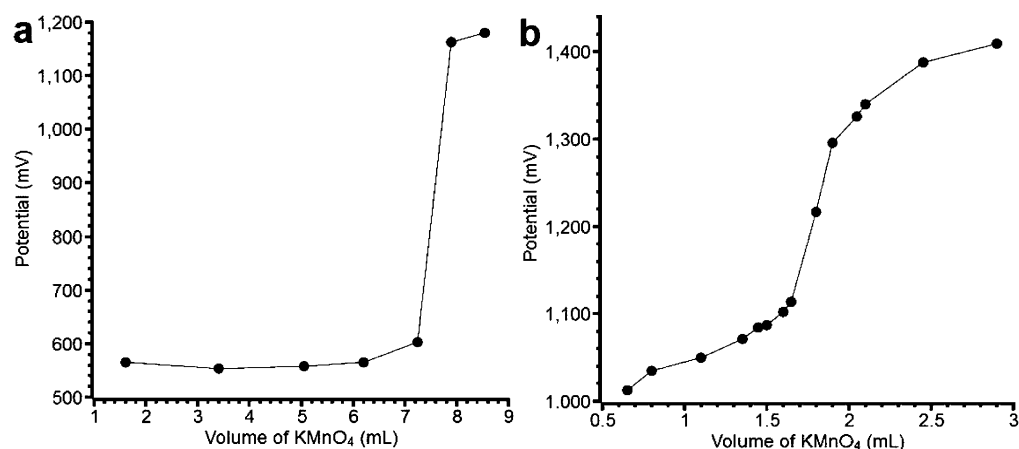


Figure 6. Manganometric redox titration curves of (a) $\text{H}_2\text{C}_2\text{O}_4 \cdot 2\text{H}_2\text{O}$ and (b) Mo-V-Bi oxide.

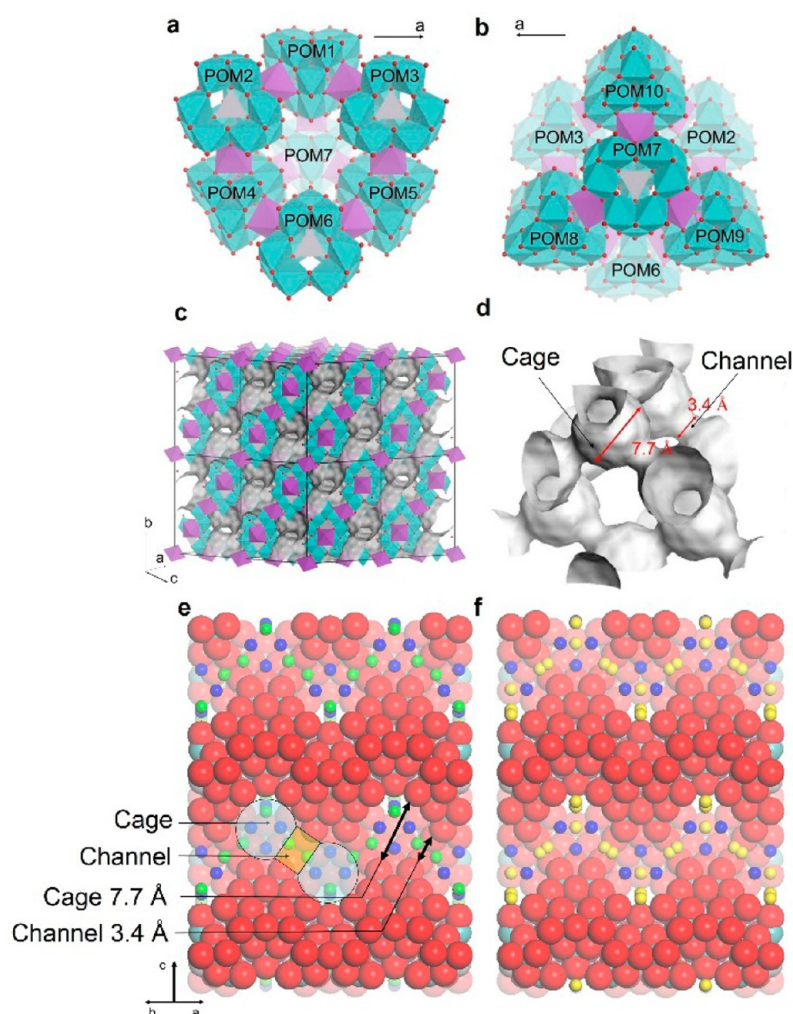


Figure 7. Polyhedral representations of (a) a front image of the cage, (b) the back image of the cage, (c) filling representation of the pore system with framework, with gray curved surface described the morepores, (d) filling representation of the pore system without framework and linkage of a cage by channels, gray curved surface described the morepores (central V, gray; Bi, purple; Mo or V, blue; O, red), (e) CPK (Corey, Pauling, and Koltun) representations of the (110) plane of Mo-V-Bi oxide (N or O in cage, blue; N or O in channel, green), and (f) K-Mo-V-Bi oxide. K: yellow. N or O in cage: blue.

(Supporting Information Figure S6c). The nitrogen adsorption-desorption isotherm of calcined Mo-V-Bi oxide was best described as a type I isotherm, indicating that Mo-V-Bi oxide was a microporous material (Figure 8a,b, black). The

BET surface area and pore volume of this material were calculated to be $60 \text{ m}^2/\text{g}$ and $0.0202 \text{ cm}^3/\text{g}$, respectively, which are similar to those of other reported POM-based porous materials (Supporting Information Table S4). The pore size

Table 3. Changes in Formulas by Ion-Exchange

entry	cation	formula ^a	amount of NH ₄ ⁺ per one ϵ -VMo _{9.4} V _{2.6} O ₄₀ ^b	
			NH ₄ ⁺ (W)	NH ₄ ⁺ (S)
1	before ion-exchange	(NH ₄) _{2.8} H _{0.9} [ϵ -VMo _{9.4} V _{2.6} O ₄₀ Bi ₂]	0.7	1.4
2	H ⁺	(NH ₄) _{2.1} H _{0.7} H _{0.9} [ϵ -VMo _{9.4} V _{2.6} O ₄₀ Bi ₂]	0	1.6
3	Li ⁺	(NH ₄) _{2.6} Li _{0.2} H _{0.9} [ϵ -VMo _{9.4} V _{2.6} O ₄₀ Bi ₂]	0.3	1.4
4	Na ⁺	(NH ₄) _{2.2} Na _{0.6} H _{0.9} [ϵ -VMo _{9.4} V _{2.6} O ₄₀ Bi ₂]	0.2	1.4
5	K ⁺	(NH ₄) _{0.9} K _{1.9} H _{0.9} [ϵ -VMo _{9.4} V _{2.6} O ₄₀ Bi ₂]	0.6	0
6	Rb ⁺	(NH ₄) _{0.7} Rb _{2.1} H _{0.9} [ϵ -VMo _{9.4} V _{2.6} O ₄₀ Bi ₂]	0.2	0
7	Cs ⁺	(NH ₄) _{0.8} Cs _{2.0} H _{0.9} [ϵ -VMo _{9.4} V _{2.6} O ₄₀ Bi ₂]	0.3	0

^aEstimated by elemental analysis. ^bEstimated by TPD.

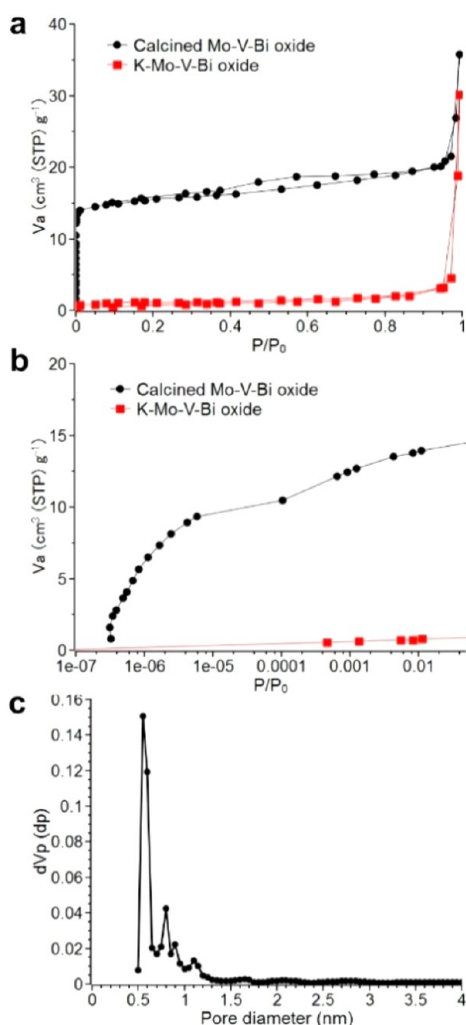


Figure 8. Nitrogen adsorption–desorption isotherms: (a) P/P_0 0–1, (b) low P/P_0 range. Black: calcined Mo–V–Bi oxide. Red: K–Mo–V–Bi oxide. (c) Pore size distribution of calcined Mo–V–Bi oxide using the SF method.

distribution curve (obtained by the SF method) showed that the average diameter of the micropores was 5.5 Å, attributed to the cages and channels in the framework (Figure 8c). The

powder XRD pattern of the material after adsorption measurement showed that the structure of the material did not change, indicating that the framework was stable under the measurement conditions.

Mo–V–Bi oxide selectively adsorbed different molecules depending on the size of the molecule (Figure 9). The size of

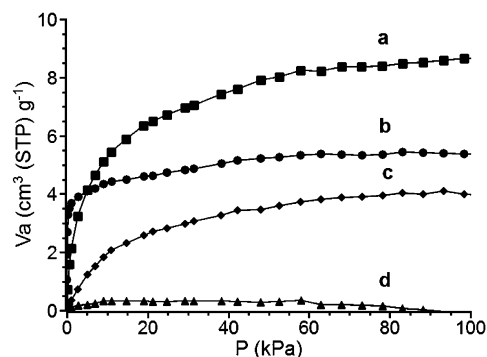


Figure 9. Molecule adsorption isotherms of Mo–V–Bi oxide (a) CO₂, (b) C₂H₆, (c) CH₄, and (d) C₃H₈.

the channel (3.4 Å) of Mo–V–Bi oxide was similar to that of C (3.4 Å) and O (3.04 Å) atoms. Therefore, the straight molecules (CO₂, CH₄, and C₂H₆), in which skeleton atoms (C and O) were in a straight line, were able to pass the channel and adsorbed in the material. C₃H₈ whose carbon skeleton was bent and larger than the channel was not adsorbed. Interestingly, Mo–V–Bi oxide adsorbed C₂H₆ at low pressure from 0.002 to 0.06 kPa (type I isotherm, Figure 9b). The theoretical accessible space of a cage (49.84 Å³) was similar to the volume of a C₂H₆ (47.28 Å³) molecule, so that C₂H₆ could fit in the cage, which may be the reason for the type I adsorption of C₂H₆.

Ion-Exchange. The ammonium cation in the micropores was exchangeable with other cations in aqueous solution, such as H⁺, Li⁺, Na⁺, K⁺, Rb⁺, and Cs⁺ (corresponding materials designated as M–Mo–V–Bi oxide, M = H, Li, Na, K, Rb, and Cs). The powder XRD patterns showed that the basic structure of ion-exchanged Mo–V–Bi oxide did not change (Supporting Information Figure S6d–g,i,j). Table 3 summarizes the formulas and amounts of NH₄⁺(S) and NH₄⁺(W) after ion-exchange estimated by elemental analysis and TPD, respectively. Moreover, TPD profiles ($m/z = 16$ for NH₃) of exchanged Mo–V–Bi oxide indicated that smaller cations such as H⁺, Li⁺, and Na⁺ selectively replaced the weakly bound ammonium cation NH₄⁺(W), whereas larger K⁺, Rb⁺, and Cs⁺ cations selectively replaced the strongly bound ammonium cation NH₄⁺(S) (Supporting Information Figure S7d–j).

In K–Mo–V–Bi oxide, in which only NH₄⁺(S) was exchanged, ca. 1.9 NH₄⁺ per one ϵ -VMo_{9.4}V_{2.6}O₄₀ building block were exchanged with K⁺. In the case of H–Mo–V–Bi oxide, in which only NH₄⁺(W) was exchanged, ca. 0.7 NH₄⁺ per one ϵ -VMo_{9.4}V_{2.6}O₄₀ building block were exchanged with H⁺. From this result, we estimated the ratio of NH₄⁺(W) and NH₄⁺(S) to be ca. 0.7–0.9:1.9–2.1. Single crystal analysis of K–Mo–V–Bi oxide revealed that 89% of K⁺ selectively occupied the channel and that the remaining 11% of K⁺, NH₄⁺, and H₂O occupied the cage in K–Mo–V–Bi oxide (Figure 7f). Therefore, we speculate that K⁺ replaced NH₄⁺ in the channel and that the NH₄⁺(S) was located in the channel and NH₄⁺(W) was located in the cage. The K⁺ blocked the

micropores of Mo–V–Bi oxide and could not be removed by calcination. The material lost microporosity with decrease in BET surface area ($4.4 \text{ m}^2/\text{g}$) after ion-exchange with K^+ (Figure 8a, red).

Activity as an Acid Catalyst. Removal of NH_3 from $\text{NH}_4^+(\text{W})$ and $\text{NH}_4^+(\text{S})$ produced weak and strong H^+ acid sites on the Mo–V–Bi oxide, respectively. Table 4 shows

Table 4. Benzyl Alcohol Dehydration To Form Dibenzyl Ether Catalyzed by Mo–V–Bi Oxide^a

entry	catalyst	conv (%)	yield (%)	sel (%)
1	as-synthesized Mo–V–Bi oxide	3	3	100
2	calcined Mo–V–Bi oxide at 623 K	95	94	99
3	calcined Mo–V–Bi oxide at 473 K	92	91	99
4	H–Mo–V–Bi oxide	99	95	95 ^b
5	recovered catalyst in entry 2	100	97	97
6	calcined Mo–V–Bi oxide at 673 K	98	91	93 ^c
7	no catalyst	5	0	0

^aReaction conditions: 20 mg of Mo–V–Bi oxide, 10 mmol of benzyl alcohol, 403 K, 3 h. After the reaction, 4 mmol of tridecane was added as an internal standard. ^bApproximately 3% of benzaldehyde was formed. ^cApproximately 4% of benzaldehyde was formed.

results of catalytic performance of Mo–V–Bi oxide for benzyl alcohol etherification. Mo–V–Bi oxide without calcination was not active (entry 1). Calcined Mo–V–Bi oxide showed catalytic activity (entry 2). Mo–V–Bi oxide calcined at temperatures over 473 K (entries 2 and 3), and proton-exchanged H–Mo–V–Bi oxide (entry 4) showed catalytic activity. These results indicated that a weak acid had sufficient catalytic activity for this reaction. Filtration experiments (Figure 10) showed that calcined Mo–V–Bi oxide was a heterogeneous

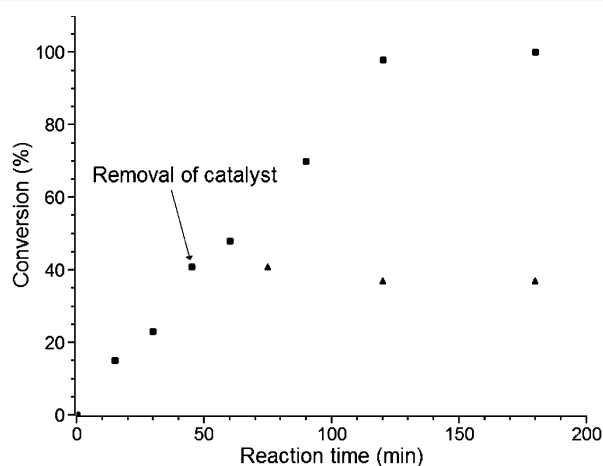


Figure 10. Filtration experiment on calcined (at 623 K) Mo–V–Bi oxide. Squares presented the reaction with catalyst. Triangles presented the reaction after removal of catalyst.

catalyst. The material could be reused without loss of activity (entry 5). The XRD pattern and IR of the recovered catalyst (Supporting Information Figure S8) confirmed high stability of Mo–V–Bi oxide during catalytic reaction. Benzyl alcohol was larger than the pore size; thus, the reaction occurred on the surface of Mo–V–Bi oxide. Therefore, Mo–V–Bi oxide calcined at 673 K, which did not contain micropores (Supporting Information Figure S9), was also active (entry 6). However, Mo–V–Bi oxide showed higher conversion of

benzyl alcohol, and the yield of dibenzyl ether compared to other reported heterogeneous catalysts (Supporting Information Table S5), which indicates that Mo–V–Bi oxide has high potential as an acid catalyst.

CONCLUSION

The first all-inorganic Keggin-type polyoxometalate-based microporous material with intrinsically ordered open micropores, Mo–V–Bi oxide, was successfully synthesized and characterized. Structural characterization showed that the material constructed by assembly of ϵ -Keggin POMs with Bi^{III} ions in a tetrahedral fashion. Heat treatment can remove the existing NH_4^+ and H_2O from the material to open the 3D micropores. The 3D micropore system of Mo–V–Bi oxide resulted from cages and channels in the material. Mo–V–Bi oxide exhibited zeolite-like properties such as molecule adsorption, ion-exchange, and acid catalysis. POMs have a diversity of elements, and they can incorporate other metals in the structure. We believe our results will open a door for production of new porous materials based on ϵ -Keggin-type POM building blocks with tunable properties.

ASSOCIATED CONTENT

Supporting Information

Detailed experimental procedures, including figures and tables. Crystallographic data in CIF format. This material is available free of charge via the Internet at <http://pubs.acs.org>.

AUTHOR INFORMATION

Corresponding Authors

*E-mail: sadakane09@hiroshima-u.ac.jp. Phone: +81-82-424-4456. Fax: +81-82-424-5494.

*E-mail: ueda@cat.hokudai.ac.jp. Phone: +81-11-706-9164. Fax: +81-11-706-9163.

Author Contributions

All authors have given approval to the final version of the manuscript.

Funding

Notes

The authors declare no competing financial interest.

ACKNOWLEDGMENTS

This work was financially supported by a Grant-in-Aid for Scientific Research (A) (Grant 2324-6135) from the Ministry of Education, Culture, Sports, Science, and Technology, Japan. The synchrotron radiation experiments were performed at the BL40XU of SPring-8 with the approval of the Japan Synchrotron Radiation Research Institute (JASRI) (Proposal 2011B1181, 2012A1161, and 2012B1110). M.S. thanks PRESTO, JST, for financial support.

REFERENCES

- (1) Special thematic issue on polyoxometalates. *Chem. Rev.* **1998**, *98*, 1–390.
- (2) Special thematic issue on polyoxometalates. *Chem. Soc. Rev.* **2012**, *41*, 7325–7648.
- (3) Long, D.-L.; Tsunashima, R.; Cronin, L. *Angew. Chem., Int. Ed.* **2010**, *49*, 1736–1758.
- (4) Kamiya, Y.; Sadakane, M.; Ueda, W. *Heteropoly Compounds*. In *Comprehensive Inorganic Chemistry II*; Reedijk, J., Poeppelmeier, K., Ed.; Oxford: Elsevier, 2013; Vol. 7, pp 185–204.

- (5) Song, J.; Luo, Z.; Britt, D. K.; Furukawa, H.; Yaghi, O. M.; Hardcastle, K. I.; Hill, C. L. *J. Am. Chem. Soc.* **2011**, *133*, 16839–16846.
- (6) Sun, C.-Y.; Liu, S.-X.; Liang, D.-D.; Shao, K.-Z.; Ren, Y.-H.; Su, Z.-M. *J. Am. Chem. Soc.* **2009**, *131*, 1883–1888.
- (7) Mizuno, N.; Misono, M. *Chem. Rev.* **1998**, *98*, 199–218.
- (8) Taylor, D. B.; McMonagle, J. B.; Moffat, J. B. *J. Colloid Interface Sci.* **1985**, *108*, 278–284.
- (9) Okamoto, K.; Uchida, S.; Ito, T.; Mizuno, N. *J. Am. Chem. Soc.* **2007**, *129*, 7378–7384.
- (10) Inumaru, K. *Catal. Surv. Asia* **2006**, *10*, 151–160.
- (11) Uchida, S.; Mizuno, N. *Coord. Chem. Rev.* **2007**, *251*, 2537–2546.
- (12) Eguchi, R.; Uchida, S.; Mizuno, N. *J. Phys. Chem. C* **2012**, *116*, 16105–16110.
- (13) Eguchi, R.; Uchida, S.; Mizuno, N. *Angew. Chem., Int. Ed.* **2012**, *51*, 1635–1639.
- (14) Jiang, C.; Lesbani, A.; Kawamoto, R.; Uchida, S.; Mizuno, N. *J. Am. Chem. Soc.* **2006**, *128*, 14240–14241.
- (15) Kawamoto, R.; Uchida, S.; Mizuno, N. *J. Am. Chem. Soc.* **2005**, *127*, 10560–10567.
- (16) Uchida, S.; Hikichi, S.; Akatsuka, T.; Tanaka, T.; Kawamoto, R.; Lesbani, A.; Nakagawa, Y.; Uehara, K.; Mizuno, N. *Chem. Mater.* **2007**, *19*, 4694–4701.
- (17) Sadakane, M.; Yamagata, K.; Kodato, K.; Endo, K.; Toriumi, K.; Ozawa, Y.; Ozeki, T.; Nagai, T.; Matsui, Y.; Sakaguchi, N.; Pyrz, W. D.; Buttrey, D. J.; Blom, D. A.; Vogt, T.; Ueda, W. *Angew. Chem., Int. Ed.* **2009**, *48*, 3782–3786.
- (18) Sadakane, M.; Endo, K.; Kodato, K.; Ishikawa, S.; Murayama, T.; Ueda, W. *Eur. J. Inorg. Chem.* **2013**, 1731–1736.
- (19) Sadakane, M.; Kodato, K.; Kuranishi, T.; Nodasaka, Y.; Sugawara, K.; Sakaguchi, N.; Nagai, T.; Matsui, Y.; Ueda, W. *Angew. Chem., Int. Ed.* **2008**, *47*, 2493–2496.
- (20) Müller, A.; Krickemeyer, E.; Bögge, H.; Schmidtman, M.; Peters, F. *Angew. Chem., Int. Ed.* **1998**, *37*, 3359–3363.
- (21) Müller, A.; Todea, A. M.; van Slageren, J.; Dressel, M.; Bögge, H.; Schmidtman, M.; Luban, M.; Engelhardt, L.; Rusu, M. *Angew. Chem., Int. Ed.* **2005**, *44*, 3857–3861.
- (22) Konya, T.; Katou, T.; Murayama, T.; Ishikawa, S.; Sadakane, M.; Buttrey, D.; Ueda, W. *Catal. Sci. Technol.* **2013**, *3*, 380–387.
- (23) Kubo, J.; Watanabe, N.; Ueda, W. *Chem. Eng. Sci.* **2008**, *63*, 1648–1653.
- (24) Watanabe, N.; Ueda, W. *Ind. Eng. Chem. Res.* **2006**, *45*, 607–614.
- (25) Sadakane, M.; Watanabe, N.; Katou, T.; Nodasaka, Y.; Ueda, W. *Angew. Chem., Int. Ed.* **2007**, *46*, 1493–1496.
- (26) Wang, F.; Ueda, W. *Catal. Today* **2009**, *144*, 358–361.
- (27) Wang, F.; Ueda, W. *Top. Catal.* **2008**, *50*, 90–97.
- (28) Sadakane, M.; Ohmura, S.; Kodato, K.; Fujisawa, T.; Kato, K.; Shimidzu, K.; Murayama, T.; Ueda, W. *Chem. Commun.* **2011**, *47*, 10812–10814.
- (29) Kaveevivitchai, W.; Jacobson, A. J. *Chem. Mater.* **2013**, *25*, 2708–2715.
- (30) Liu, D.; Lu, Y.; Tan, H.-Q.; Chen, W.-L.; Zhang, Z.-M.; Li, Y.-G.; Wang, E.-B. *Chem. Commun.* **2013**, *49*, 3673–3675.
- (31) Mitchell, S. G.; Streb, C.; Miras, H. N.; Boyd, T.; Long, D.-L.; Cronin, L. *Nat. Chem.* **2010**, *2*, 308–312.
- (32) Mitchell, S. G.; Boyd, T.; Miras, H. N.; Long, D.-L.; Cronin, L. *Inorg. Chem.* **2011**, *50*, 136–143.
- (33) Mandic, S.; Healey, M. R.; Gotthardt, J. M.; Alley, K. G.; Gable, R. W.; Ritchie, C.; Boskovic, C. *Eur. J. Inorg. Chem.* **2013**, *2013*, 1631–1634.
- (34) Nohra, B.; El Moll, H.; Rodriguez Albelo, L. M.; Mialane, P.; Marrot, J.; Mellot-Draznieks, C.; O’Keeffe, M.; Biboum, R. N.; Lemaire, J.; Keita, B.; Nadjjo, L.; Dolbecq, A. *J. Am. Chem. Soc.* **2011**, *133*, 13363–13374.
- (35) Rodriguez-Albelo, L. M.; Rabdel Ruiz-Salvador, A.; Sampieri, A.; Lewis, D. W.; Gomez, A.; Nohra, B.; Mialane, P.; Marrot, J.; Secheresse, F.; Mellot-Draznieks, C.; Biboum, R. N.; Keita, B.; Nadjjo, L.; Dolbecq, A. *J. Am. Chem. Soc.* **2009**, *131*, 16078–16087.
- (36) Dolbecq, A.; Mialane, P.; Secheresse, F.; Keita, B.; Nadjjo, L. *Chem. Commun.* **2012**, *48*, 8299–8316.
- (37) Müller, A.; Beugholt, C.; Kogerler, P.; Bogge, H.; Bud’ko, S.; Luban, M. *Inorg. Chem.* **2000**, *39*, 5176–5177.
- (38) Mialane, P.; Dolbecq, A.; Lisnard, L.; Mallard, A.; Marrot, J.; Secheresse, F. *Angew. Chem., Int. Ed.* **2002**, *41*, 2398–2401.
- (39) Sloboda-Rozner, D.; Neimann, K.; Neumann, R. *J. Mol. Catal. A: Chem.* **2007**, *262*, 109–113.
- (40) Tucher, J.; Nye, L. C.; Ivanovic-Burmazovic, I.; Notarnicola, A.; Streb, C. *Chem.—Eur. J.* **2012**, *18*, 10949–10953.
- (41) Baur, W. H. *Am. Mineral.* **1964**, *49*, 697–704.
- (42) Suib, S. L. *Acc. Chem. Res.* **2008**, *41*, 479–487.
- (43) Suib, S. L. *J. Mater. Chem.* **2008**, *18*, 1623–1631.
- (44) Fyfe, C. A.; Gies, H.; Kokotailo, G. T.; Marler, B.; Cox, D. E. *J. Phys. Chem.* **1990**, *94*, 3718–3721.
- (45) Young, R. A. *The Rietveld Method*; Young, R. A., Ed.; Oxford University Press: Oxford, 1995.
- (46) Ryu, J.; Park, R.; Kim, D.-S. *J. Comput. Sci. Technol.* **2006**, *21*, 225–260.
- (47) Yasuda, N.; Fukuyama, Y.; Toriumi, K.; Kimura, S.; Takata, M. Submicrometer Single Crystal Diffractometry for Highly Accurate Structure Determination. In *AIP Conference Proceedings*; Garrett, R., Gentle, I., Nugent, K., Wilkins, S., Eds.; 2010; Vol. 1234, pp 147–150.
- (48) Yasuda, N.; Murayama, H.; Fukuyama, Y.; Kim, J.; Kimura, S.; Toriumi, K.; Tanaka, Y.; Moritomo, Y.; Kuroiwa, Y.; Kato, K.; Tanaka, H.; Takata, M. *J. Synchrotron Radiat.* **2009**, *16*, 352–357.
- (49) Sheldrick, G. M. *SHELX-97, Program for Crystal Structure Analysis*; Universität Göttingen: Göttingen, Germany, 1997.
- (50) Zhang, Q.-Z.; Lu, C.-Z.; Yang, W.-B.; Wu, C.-D.; Yu, Y.-Q.; Yan, Y.; Liu, J.-H.; He, X. *J. Cluster Sci.* **2003**, *14*, 381–390.
- (51) Zang, X.; Tan, H.; Wu, Q.; Li, Y.; Li, Y.; Wang, E. *Inorg. Chem. Commun.* **2010**, *13*, 471–474.
- (52) Chae, K.; Day, V. W.; Eberspacher, T. A. *Inorg. Chem.* **1992**, *8*, 3187–3189.